ISSN 0036-0236, Russian Journal of Inorganic Chemistry, 2019, Vol. 64, No. 6, pp. 742–754. © Pleiades Publishing, Ltd., 2019.

COORDINATION COMPOUNDS

Soluble Cytotoxic Ruthenium(II) Complexes with 2-Hydrazinopyridine

A. A. Soliman[a], *, F. A. Attaby[a], O. I. Alajrawy[b], S. R. Majeed[a], C. Sahin[c], and C. Varlikli[d]

[a] *Department of Chemistry, Faculty of Science, Cairo University, Giza, 12613 Egypt*

[b] *Department of Applied Chemistry, College of Applied Science, University of Fallujah, Fallujah, Anbar, Iraq*

[c] *Department of Chemistry, Art and Science Faculty, Pamukkale University, Denizli, Turkey*

[d] *Department of Photonics, Izmir Institute of Technology, Urla-Izmir, 35430 Turkey*

**e-mail: ahmedsoliman61@gmail.com*

Received June 4, 2018; revised August 21, 2018; accepted November 27, 2018

Abstract– New water soluble Ru(II) binary complex $[Ru(C_5H_7N_3)(X)(H_2O)_2]$ with 2-hydrazinopyridine and its ternary complexes with X = dichloride, oxalate, malonate or pyrophosphate ligands have been synthesized. The complexes have been characterized using elemental analyses, mass, IR, and UV-Vis. spectroscopies, cyclic voltammetry, magnetic susceptibility, and thermal analysis. The complexes are diamagnetic and the electronic spectral data showed that peaks are due to low spin octahedral Ru(II) complexes. The optimized structures of the complexes **1**–**4** indicate distorted octahedral geometry with bond angles around the ruthenium atom ranged from 80.44° to 99.64°. The values of the electronic energies (–635 to –1145 a.u.), the highest occupied molecular orbital energies (–0.181 to 0.073 a.u.) and lowest unoccupied molecular orbital energies (–0.056 to 0.167 a.u.) indicate the stability of the complexes. The complexes are polarized as indicated from the dipole moment values (9.39–14.27 Debye). The complexes have noticeable cytotoxicity with IC_{50} (μM): 0.011–0.062 (HepG-2), 0.015–0.080 (MCF-7), 0.015–0.116 (HCT-116), and PC-3 (0.034–0.125).

Keywords: Ru(II) complexes, 2-hydrazinopyridine, antitumor complexes, Cytotoxicity, DFT calculations

DOI: 10.1134/S0036023619060020

INTRODUCTION

The toxic side effects of cisplatin and the limitation of activity against wide spectrum of cell lines with its second generation (oxaliplatin) and third generation (carboplatin) motivate the researchers to design and prepare innovative metal-based anticancer drugs [1–2]. The most important point is improving the strategy of the targeting by designing metal-based complexes with ligands to increase cellular uptake and selectivity of the drugs against the cancer cells [3–5]. The main reason encouraging the chemists to design and prepare ruthenium complexes as a chemotherapeutic agent is the high selectivity for cancer cells [6]. In addition, ruthenium has unique properties, namely: mimic to iron can bind to serum transferrin and albumin, considered as pro-drug by reduction from the inert oxidation state Ru(III) to more active oxidation state Ru(II) in tumor tissue and this gives selective toxicity, slow ligand exchange kinetics and the ability to bind to DNA [7, 8]. Because of the octahedral geometry, ruthenium has been used to build effective chemotherapeutic agents which have lower side effects and more selective than platinum complexes; they have been examined as DNA topoisomerase inhibitors [9–17]. The most extensively studied ruthenium compounds were the ruthenium polypyridyl which showed attractive antitumor cytotoxicity. These complexes were inducing the apoptosis of the cancer cells [18].

The important ruthenium complex, RAPTA-C $[Ru(\eta^6\text{-}p\text{-cymene})Cl_2(1,3,5\text{-triaza-7-phosphaadamantane})]$ has been shown to possess interesting clinical properties when the complex is applied in combination with other drugs and gives good inhibition of tumor growth without side effects and very low doses. The complex RDC11 [Ru(phenanthroline)(κ-C,N-(2-phenyl-pyridine)$(NCMe)_2]PF_6$ showed similar tumor reduction compared to cisplatin on the tumor volume when tested against xenografted A2780 ovarian cancer cells and U87 glioblastoma cells. The complex $[Ru(\eta^6\text{-arene})(ethylenediamine)Cl]^+$ showed promising anticancer properties in different in vivo models [8, 19, 20]. The kinetics of ligand exchange of metal complexes is the crucial step of hydrolysis in aqueous solution, hence, of complexes cytotoxicity. The hydrolysis of ruthenium complexes is very close to the value of platinum complexes [21]. Several ruthenium complexes have been prepared and used as alternatives for platinum complexes in chemotherapy. Ruthenium bipyridyl complexes don't accumulate in the nucleus and their cellular uptake occurs either by

endocytosis or by active transport depending on the structure of the complex. For example, [Ru(2,2'-bipyridine)$_2$Cl$_2$] is inactive, whereas [Ru(2,2',6',2''-terpyridine)Cl$_3$] has good cytotoxicity against the murine and human cancer cell lines [21]. In Continuation to our work on antitumor metal complexes [22–24], we report here four Ru(II) complexes with 2-hydrazinopyridine ligand as the diamine moiety and either chloride, oxalate, malate or pyrophosphate ligands as the labile group. The structures of ligands used in this study are shown in Scheme 1.

EXPERIMENTAL

Materials. The chemicals used are highly pure. Ruthenium(III) chloride monohydrate $RuCl_3 \cdot H_2O$, 2-hydrazinopyridine hydrochloride $C_5H_7N_3$, potassium oxalate monohydrate $K_2C_2O_4 \cdot H_2O$, malonic acid $CH_2(COOH)_2$, and sodium pyrophosphate decahydrate $Na_4P_2O_7 \cdot 10H_2O$ were supplied by Aldrich; tetrabutyl ammonium hexafluorophosphate $TBAPF_6$ was purchased from Fluka. All solvents were of analytical grade.

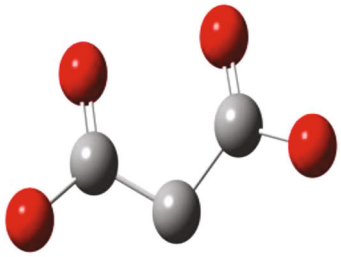

$C_3H_2O_4^{2-}$ malonate

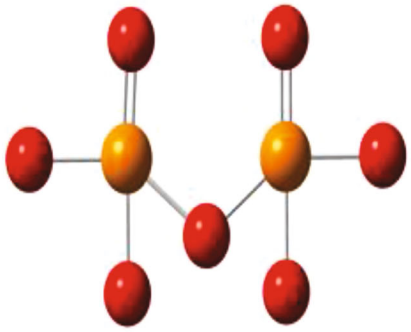

$P_2O_7^{4-}$ pyrophosphate

Scheme 1. Structures of the ligands used in this study.

Measurements. The elemental analysis for carbon, hydrogen, and nitrogen was carried out at the microanalytical laboratory of Cairo University, Egypt. Electrochemical data were obtained by using a CH Instrument 660 B Model Electrochemical Workstation. IR measurements of the solid complexes were carried out as KBr pellets using Jasco FTIR-460 plus and Jasco FTIR-4000 (range 400–4000 cm^{-1}); mass-spectral measurements were conducted using a GCMS-QP 1000EX Shimadzu device. UV-Vis spectra were recorded in a 1 cm path length quartz cell by using an Optizen UV-Vis spectrophotometer. The magnetic susceptibility measurements of the solid complexes were carried out using a Sherwood Scientific, Cambridge Science Park Cambridge-England magnetic susceptibility balance. Thermal analysis was carried out using a Shimadzu thermo-gravimetric analyzer TGA-60H; under a nitrogen atmosphere (20 mL/min) with a heating rate of 10 K/min over a temperature range from room temperature up to 1000°C.

MO calculations were carried out using the GAUSSIAN 09W software. The geometries of the singlet ground state of complexes were fully optimized in the gas phase at the B3LYP/LanL2DZ basis set.

Preparation of complexes 1–4. 2-Hydrazinopyridine (0.11 g, 1.0 mmol) was dissolved separately in 10 mL of ethanol and slightly added to $RuCl_3.H_2O$ (0.21 g, 1.0 mmol) in water (10 mL). The mixture was adjusted to pH 3.5 and refluxed at 90°C for 4 h under constant stirring to get complex **1**. Complex **2** has been prepared by the addition of potassium oxalate monohydrate $K_2C_2O_4 \cdot H_2O$ (0.18 g, 1.0 mmol) to a solution of 2-hydrazinopyridine ligand and ruthenium salt while stirring. Similarly, complexes **3** and **4** have been prepared by the addition of malonic acid $H_2C_3H_2O_4$ (0.10 g, 1.0 mmol) and sodium pyrophosphate decahydrate $Na_4P_2O_7 \cdot 10H_2O$ (0.45 g, 1.0 mmol), respectively. The complexes were obtained as deep-violet precipitates. Yield, 76.3 (**1**), 73.2 (**2**), 77.6 (**3**), and 71.4% (**4**).

For **1** ($C_5H_{11}Cl_2N_3O_2Ru$) anal. calcd. (%): C, 18.94; H, 3.50; N, 13.25. Found (%): C, 18.87; H, 3.38; N, 13.16; mp > 300°C;

For **2** ($C_7H_{11}N_3O_6Ru$) anal. calcd. (%): C, 25.15; H, 3.32; N, 12.57. Found (%): C, 24.99; H, 3.27; N, 12.84; mp > 300°C.

For **3** ($C_8H_{13}N_3O_6Ru$) anal. calcd. (%): C, 27.59; H, 3.76; N, 12.07. Found (%): C, 27.42; H, 3.58; N, 11.89; mp > 300°C.

For **4** ($C_5H_{13}N_3O_9P_2Ru$) anal. calcd. (%): 14.22; H, 3.10; N, 9.95. Found (%): C, 14.17; H, 3.05; N, 9.78; mp > 300°C.

In vitro antitumor activity. The cytotoxicity tests were carried out using the rapid colorimetric assay for cellular growth and survival [25]. The human tumor

Table 1. Analytical and spectral data of the Ru(II) complexes prepared

Complex	Molar mass	m/z (P^+)	Λ_m, Ω^{-1} cm^2 mol^{-1}	UV-V is absorption peaks, nm	
$[Ru(C_5H_7N_3)Cl_2(H_2O)_2]$ (**1**)	317.14	318	1.43	310 380 470–560	$\pi \rightarrow \pi^*$ $n \rightarrow \pi^*$ LMCT
$[Ru(C_5H_7N_3)(C_2O_4)(H_2O)_2]$ (**2**)	334.24	334	3.31	300 360 460–580	$\pi \rightarrow \pi^*$ $n \rightarrow \pi^*$ LMCT
$[Ru(C_5H_7N_3)(C_3H_2O_4)(H_2O)_2]$ (**3**)	348.28	349	2.65	310 370 460–560	$\pi \rightarrow \pi^*$ $n \rightarrow \pi$ LMCT
$[Ru(C_5H_7N_3)(H_2P_2O_7)(H_2O)_2]$ (**4**)	422.20	424	4.20	300 360 460–580	$\pi \rightarrow \pi^*$ $n \rightarrow \pi^*$ LMCT

* LMCT: $\nu_2(\pi L \rightarrow Meg(\sigma^*))$, ν_4 $(\sigma L \rightarrow Meg(\sigma^*))$.

cells used are hepatocellular cancer cell line (HepG-2), breast cancer cell line (MCF-7), colon carcinoma cell line (HCT-116), and prostate carcinoma cell line (PC-3) to test the cytotoxicity of the complexes under study. The tumor cells were cultured in Dulbecco's modified Eagle's medium (DMEM) or RPMI-1640 depending on the type of cell line supplemented with 10% heat-inactivated fetal bovine serum, 1% L-glutamine, HEPES buffer and 50 μg/mL gentamycin. The cells were incubated at 37°C in a humidified atmosphere with 5% CO_2 and were subcultured two times a week along the experimentation. Each experiment has been carried out in triplicate. The cytotoxicity test was carried out in the Regional Centre for Mycology and Biotechnology Al-Azhar University, Cairo, Egypt.

RESULTS AND DISCUSSION

The analytical and spectral data of the prepared ruthenium complexes **1**–**4** are given in Table 1. The complexes are air stable and soluble in water. It is worth to mention that Ru(III) has been reduced to Ru(II) during the complex formation and this is consistent with the reported amine and phosphine complexes such as $[Ru(bipy)_3]Cl_2]$ [26], $[RuCl_2(PPh_3)_3]$ [27], $[Ru(tpy)(bpy)(4\text{-}NH_2\text{-}py)](PF_6)_2]$ [28], $[Ru(phen)_2Cl_2] \cdot 2H_2O$ [29], $[Ru(bipy)(DABA)(NCS)_2]$, and $[Ru(hzpy)(DABA)(NCS)_2]$ [30] have been reported to reduce Ru(III) to Ru(II) which is stabilized by complexation.

IR Spectra

The experimental and calculated IR peaks of the Ru(II) complexes prepared are given in Table 2. The ν(N–H) stretching vibrations peak of the amino groups of 2-hydrazinopyridine at 3305–3256 cm^{-1} in the ligand spectrum has been appeared in the spectra of all complexes as merged broad bands being shifted to the range 3427–3431 cm^{-1} indicating the NH_2 groups to participate in coordination [31]. The coordination of the NH_2 groups has been also confirmed by the shift of the bending vibrations found at 1159–1250, 1075–1154, and 768–776 cm^{-1} assigned for the stretching vibrations (ρtNH_2), (ρwNH_2), and (ρrNH_2), respectively. The spectra of complexes **2** and **3** showed new additional bands at 1642 and 1626 cm^{-1}, respectively, which assigned for the stretching vibrations ν(C=O). The asymmetric and the symmetric COO stretching vibrations have been found at 1511–1528 and 1301–1320 cm^{-1}, respectively [32, 33]. The difference (Δν) of the asymmetric and symmetric carbonyl stretching frequencies is larger than 200 cm^{-1}, which indicates that the two carboxylate groups of the oxalate and malonate are coordinated to ruthenium(II) in *cis*-form [34–36]. The IR spectrum of complex **4** showed bands at 1187 and 1075 cm^{-1} assigned to the asymmetric and symmetric stretching vibration of the terminal $\nu(PO_3)$, respectively. The existence of $\nu(PO_3)$ in the complex spectrum indicates that $[P_2O_7]_4^-$ ring adopts a bent configuration [18, 34–36]. The experimental and calculated IR spectra of the ligand and complexes **1**–**4** are shown in Figs. S1–S5 in SI. There is agreement between the experimental and calculated spectra as shown in Table 2. The difference between the experimental and calculated results may be explained on the basis of the different methodology used for getting the data; the experimental data are measured in the solid state while the calculated data were deduced from the isolated gaseous molecular state.

Table 2. Experimental and calculated vibrational frequencies for Ru(II) complexes, cm^{-1}

Complex	Exp.	Calc.	Assignment
2-Hydrazinopyridine	3395, 3308	3508, 3444	ν(N–H)
	1246	1299	ρtNH_2
	1086	1193	ρwNH_2
	804	856	ρrNH_2
1	3431	3535	ν(N–H)
	1249	1290	ρtNH_2
	1055	1157	ρwNH_2
	768	776	ρrNH_2
2	3430	3540	ν(N–H)
	1250	1280	ρtNH_2
	1154	1151	ρwNH_2
	776	715	ρrNH_2
	1624	1653	ν(C=O)
3	3429	3420	ν(N–H)
	1247	1263	ρtNH_2
	1115	1148	ρwNH_2
	774	721	ρrNH_2
	1626	1648	ν(C=O)
4	3427	3418	ν(N–H)
	1159	1148	ρtNH_2
	1246	1234	ρwNH_2
	775	771	ρrNH_2
	1187, 1075	1176, 1068	ν(O–P–O)
	892	881	ν(P=O)

Mass Spectral Analysis

The major fragmentations in the mass spectra of the prepared Ru(II) complexes are present in Figs. S6–S9 in SI. The spectrum of complex **1** (FW = 317.14) showed a parent peak at m/z = 318 (M^+), peaks at m/z = 281 (M-2H_2O), m/z = 209 (ML) and m/z = 110 for the 2-hydrazinopyridine ligand. The spectrum of complex **2** (FW = 334.25) gave a parent peak at m/z = 334 (M), peaks at m/z = 297 (M-2H_2O), m/z = 210 (ML), and m/z = 110 for the 2-hydrazinopyridine ligand. The spectrum of complex **3** (FW = 347.27) gave a parent peak at m/z = 349 (M^+), peaks at m/z = 313 (M-2H_2O), m/z = 217 (ML), and m/z = 110 for the 2-hydrazinopyridine ligand. The spectrum of complex **4** (FW = 422.20) gave a parent peak at m/z = 424 (M^+), peaks at m/z = 388 (M^+-2H_2O), m/z = 212 (ML), m/z = 160 ($H_2P_2O_6$), and m/z = 110 for the 2-hydrazinopyridine ligand. The spectra of complexes **1**–**4** showed also peaks at m/z 98, 99, 100, 101, and 102 which are assigned to the stable ruthenium isotopes [37].

Electrochemical Data

The electrochemical measurements were obtained by cyclic voltammetry in a cell containing glassy carbon working electrode, a Pt wire counter electrode, an Ag wire reference electrode, and supporting electrolyte, i.e. 0.1 M $TBAPF_6$ in DMF. The HOMO and LUMO energy levels of the complexes were calculated by using ferrocene (0.65 V vs. Ag/Ag^+) as the internal standard and the maxima of first oxidation and reduction potentials, respectively [38]. The obtained data were summarized in Table 3.

The cyclic voltammogram of 2-hydrazinopyridine ligand exhibited one oxidation (1.09 V) and one reduction peaks (−1.30 V) assigned to the hydrazine and pyridine parts of the ligand, respectively. The differential cyclic voltammogram of complex **1** shows one broad oxidation peak at 1.29 V which is attributed to the ruthenium metal as the main character and the contribution of 2-hydrazinopyridine ligand to the highest occupied molecular orbital (HOMO) (Fig. 1). The reduction peaks of −1.05 V and −1.70 V are attributed to the 2-hydrazinopyridine ligand and chloride, respectively. The contribution of Ru and 2-hydrazinopyridine ligand to HOMO and 2-hydrazinopyridine ligand and malate to LUMO energy states in complex **3** exhibits the same trend as complex **1**. The HOMO and LUMO energy levels of the complexes are in the range from 5.28 to 5.44 eV and 3.10 to 3.21 eV, respectively. Consecutive cyclic behaviors of the complexes presented no significant change in peak currents and potentials of anodic and cathodic areas.

Electronic Spectra

The electronic spectral measurements were recorded using the aqueous solution of complexes **1**–**4** in the 200–1100 nm range. The experimental and calculated absorption spectra of complexes **1**–**4** are shown in Figs. S10–S13 in SI. The resulted data are

Table 3. Electrochemical data of the 2-hydrazinopyridine ligand and the complexes **1** and **3** in DMF

Molecules	E_{ox1}, V	E_{red1}, V	E_{red2}, V	HOMO, eV	LUMO, eV
2-Hydrazinopyridine	1.09	−1.30	–	−5.24	−2.85
1	1.29	−1.05	−1.70	−5.44	−3.10
3	1.13	−0.94	−1.21	−5.28	−3.21

given in Table 1. The spectra showed absorption bands in the range 260–310 nm and 360–380 nm which can be assigned to the $\pi \rightarrow \pi^*$ and $n \rightarrow \pi^*$ transitions of the pyridine ring group of the 2-hydrazinopyridine ligand, respectively [39]. The spectra showed also shoulders at 460–580 nm which are due to LMCT (ligand-to-metal charge transfer) within octahedral species, $\nu_4(\sigma L \rightarrow Meg(\sigma^*))$ transition [39, 40]. It is worth to mention that both $\nu_1(\pi L \rightarrow Mt_{2g}(\pi^*))$ and $\nu_3(\sigma L \rightarrow Mt_{2g}(\pi^*))$ transitions have not been observed as the metal t_{2g} is completely filled in low spin complexes [39]. The possibility of back donation from Ru(II) to the 2-hydrazinopyridine ligand (MLCT) is also inferred from the computational studies (*vide infra*). The *d*–*d* transitions within the low spin octahedral ruthenium(II) d^6-complexes are very weak and have not been not observed because of the high intensity of the strong LMCT [39–41]. The configurations of the computed main excitation electronic transition as well as the oscillator strength of Ru(II) complexes are given in Table 4. The predicted transitions are in good agreement with the experimental values. The experimental and calculated electronic transitions for complex **4** are presented in Fig. 2; the data for complexes **1**–**3** are shown in Figs. S14–S16 in SI. The assignment of the calculated orbital excitations to the experimental bands was based on the relative HOMO and LUMO energies involved in the electronic transitions.

Magnetic Susceptibility Measurements

Magnetic susceptibility measurements of Ru(II) complexes **1**–**4** showed that all complexes are diamagnetic which can be explained on the fact that Ru(II) is divalent (d^6), ($t_{2g}{}^6e_g{}^0$) in a low spin octahedral geometry with all electrons are paired [42].

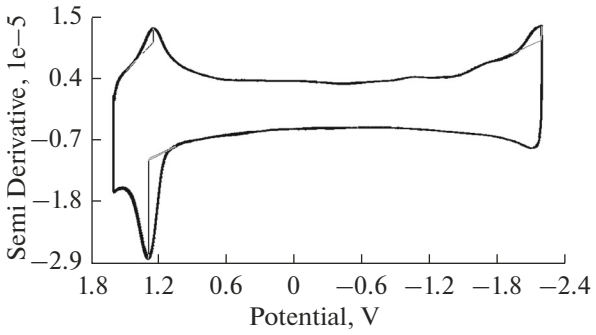

Fig. 1. Differential cyclic voltammogram of $[Ru(C_5H_7N_3)Cl_2(H_2O)_2]$ (**1**) measured in DMF solution containing 0.1 M $TBAPF_6$ with scan speed of 100 mVs^{-1}.

Thermal Studies

In order to investigate the thermal stability of complexes, the thermogravimetric analysis (TGA) of the complexes has been performed. The derivative thermogravimetric analysis (DrTGA) has been also used to describe the steps ranges with better precision. The data obtained for complexes **1**–**4** are shown in Figs. S17–S20 in SI. The TG curves of the Ru(II) complexes were carried out under nitrogen atmosphere 20 mL/min with a heating rate of 10°C/min over a temperature range from room temperature up to

Table 4. Main excitation energies (nm), electronic transition configurations, and oscillator strengths (*f*) of the Ru(II) complexes

Complex	Calcd., nm	Exp., nm	Oscillator strengths	Composition (>10%)
1	265	310	0.075	HOMO-3 → LUMO (59%), HOMO → LUMO + 5 (28%)
	359	380	0.098	HOMO-2 → LUMO (50%), HOMO-1 → LUMO (30%)
	410	470	0.009	HOMO → LUMO (44%), HOMO-2 → LUMO + 3 (38%)
2	263	300	0.079	HOMO-3 → LUMO + 1 (66%)
	328	360	0.014	HOMO-1 → LUMO + 3 (63%)
	389	460	0.105	HOMO → LUMO + 1 (46%), HOMO-2 → LUMO + 7 (28%)
	432	580	0.025	HOMO → LUMO (51%), HOMO-1 → LUMO (26%)
3	285	310	0.063	HOMO-6 → LUMO (50%), HOMO → LUMO + 4 (29%)
	367	370	0.143	HOMO-2 → LUMO + 2 (53%), HOMO-2 → LUMO + 2 (34%)
	459	460	0.025	HOMO → LUMO + 3 (34%), HOMO-1 → LUMO + 3 (34%)
	582	560	0.028	HOMO → LUMO (42%), HOMO-2 → LUMO (39%)
4	264	300	0.067	HOMO-3 → LUMO (68%)
	371	360	0.033	HOMO-1 → LUMO + 2 (66%)
	450	460	0.089	HOMO → LUMO (46%)
	460	580	0.021	HOMO-1 → LUMO + 5 (41%), HOMO-2 → LUMO (30%)

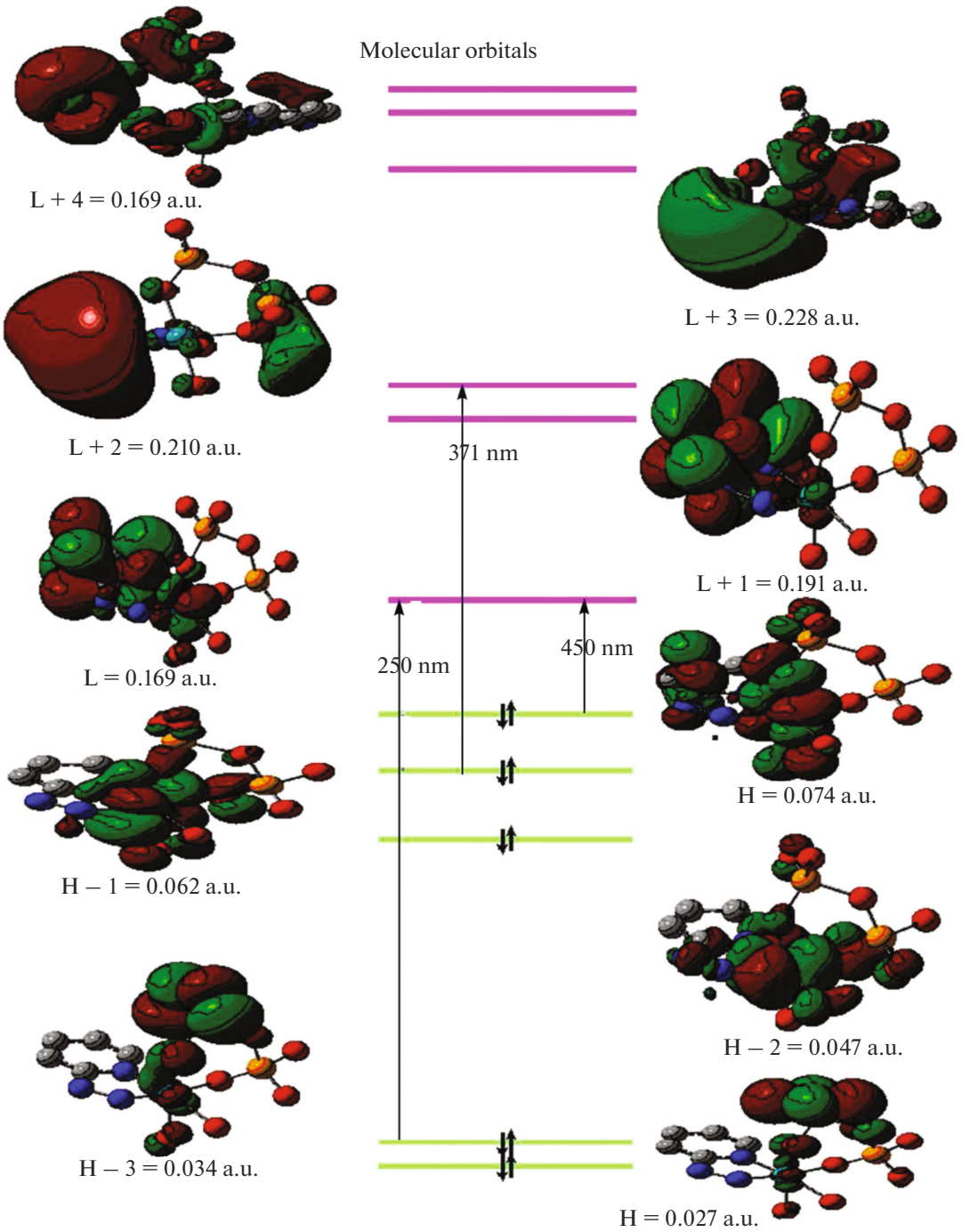

Fig. 2. The calculated electronic transition (TD-DFT/B3LYP/LANL2DZ) of $[Ru(C_5H_7N_3)(H_2P_2O_7)(H_2O)_2]$ complex **4** (isovalue = 0.02).

1000°C. All complexes have been decomposed in three steps. The first decomposition step of complex **1** has been observed at 305–511 K and is assigned to loss of two coordinated water molecules with mass loss of 11.42% (calcd. 11.32%). The second decomposition step observed at 512–833 K is assigned to loss of the ligand ($C_5H_7N_3$) with mass loss of 35.11% (calcd. 34.27%) and the last decomposition step observed at 834–1000 K is assigned to loss of two chlorides with mass losses of 23.09% (calcd. 22.32%). For complex **2**: first decomposition step, 296–393 K, loss of two coordinated water molecules with mass loss of 9.64% (calcd. 10.77%); second decomposition step, 394–504 K, loss of the ligand ($C_5H_7N_3$) with mass loss of 32.07% (calcd. 32.63%); third decomposition step, 505–998 K, loss of two carbon dioxide with mass losses of 26.61%

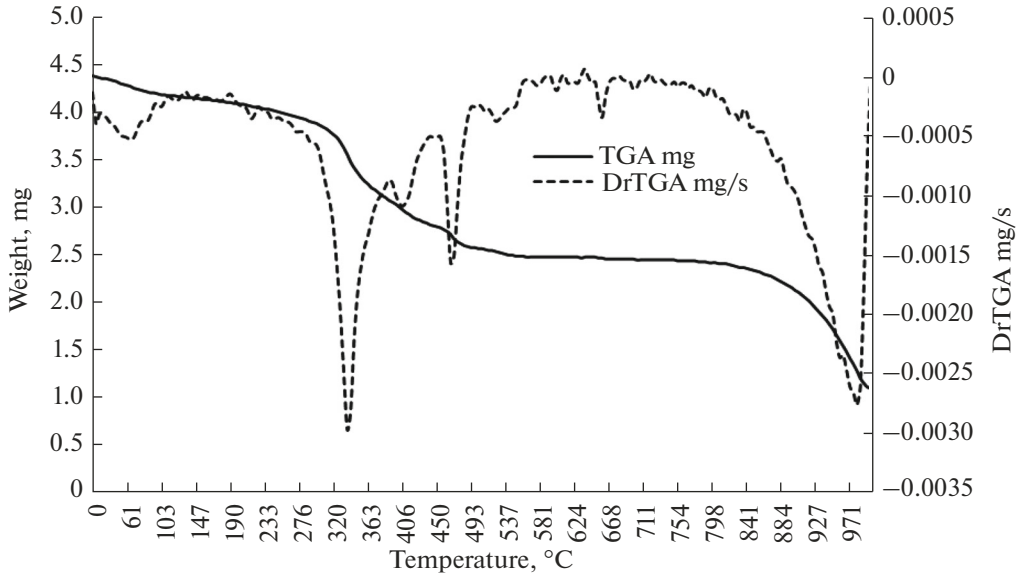

Fig. 3. TG and DTG plot of $[Ru(C_5H_7N_3)Cl_2(H_2O)_2]$ complex **1**.

(calcd. 22.37%). For complex **3**: first decomposition step, 303–466 K, loss of two coordinated water molecules with mass loss of 10.88% (calcd. 10.31%); second decomposition step, 467–551 K, loss of ligand ($C_5H_7N_3$) with mass loss of 30.17% (calcd. 31.23%); last decomposition step, 552–720 K, loss of ($C_3H_2O_4$) with mass loss of 29.88% (calcd. 29.22%). For complex **4**: first decomposition step, 295–376 K, loss of two coordinated water molecules with mass losses of 8.54% (calcd. 8.49%); second decomposition step, 459–505 K, loss of $H_2P_2O_6$ with mass loss of 37.55% (calcd. 37.73%); last decomposition step, 506–999 K, loss of $C_5H_7N_3$ with mass losses of 26.61% (calcd. 25.70%).

The residue in all complexes has found to be the metallic ruthenium with mass 30.38% (calcd. 31.76%), 25.55% (calcd. 26.34%), 29.10% (calcd. 28.93%), and 27.30% (calcd. 27.59%) for complexes **1**, **2**, **3**, and **4**, respectively [43, 44].

The thermal stability of the complexes is indicated from their relatively high overall activation energies (101–254 kJ mol^{-1}). The steps of decomposition are consistent with the proposed complexes formulae. The thermogram of complex **1** is shown in Fig. 3 as an example. The thermodynamic parameters have been calculated using the integral method, the Coats–Redfern and Approximation method, Horowitz–Metzger [45, 46] method considering the Ozawa correction [47].

The decomposition temperature ranges with mass losses are given in Table 5. The values of the thermodynamic parameters of the complexes are given in Table S1 shown in SI. The values of the entropy of the formation (ΔS^*) of Ru(II) complexes were negative in all decomposition steps which is consistent with the of structural complexity (arrangement) of the activated complexes as the starting reactants in each step [45–47].

Theoretical Studies

The energy minimization studies were carried out using the GAUSSIAN 09W software program. Molecular geometries of the singlet ground state of the complexes were fully optimized in the gas phase at the B3LYP/LanL2DZ basis set [48, 49]. The optimized geometries of complexes **1**–**4** are given in Fig. 4.

Selected bond angles and bond lengths are given in Table S2. The angles between Ru(II) and the surrounded atoms of chloride and oxygen of secondary ligands vary from (80.44° to 94.25°) and dihedral angles from (169.64° to 175.04°) which are deviated from those of perfect octahedral (90°, 180°) indicating distorted octahedral structures [50]. The Cl–Ru–Cl bond angle in complex **1** (94.25°) is comparable with the ruthenium(II) diamine dichloride complex (92.66°) in *cis*-[$RuCl_2$(dppme)(2-diaminocyclohexane)] [51]. The O–Ru–O bond angles in complexes **2** and **3** (83.30° and 82.02°); respectively arecomparable with the ruthenium (II) diamine oxalate complex (78.70°) in $[Ru(C_2O_4)(C_{10}H_{14})(C_7H_5NO_4)]$ [52].

The N–Ru–N bond angles (80.22°–81.48°) are also deviating from (90°). A comparison of the calculated Ru–Cl and Ru–N bond lengths with those of reported Ru(II) complexes involving bidentate *N*-donor ligands reveals that the average values found for Ru–Cl (2.493 Å) is consistent with the range of the reported values {2.473 (*p*-cymene)Ru(curcuminato)chloro} [49].The calculated Ru–O bond lengths values found (2.051–2.117 Å) are consistent with the range of reported values {2.083 [Ru-$(C_2O_4)(C_{10}H_{14})(C_7H_5NO_4)$]}

Table 5. Thermogravimetric decomposition data of Ru(II) complexes

Complex	FW	TG range, K	DTA_{max}, K	Mass loss, found (calcd.), %	Assignment of the removed species	Metallic residue, found/calcd.
1	317.14	305–511	406	11.42/11.32	$2H_2O$	Ru 30.38/31.76)
		512–833	611	35.11/34.27	$C_5H_7N_3$	
		834–1000	1248	23.09/22.32	Cl_2	
2	334.24	296–393	347	9.64/10.77	$2H_2O$	Ru 31.68/30.23)
		394–504	500	32.07/32.63	$C_5H_7N_3$	
		505–998	770	26.61/26.34	$2CO_2$	
3	348.28	303–466	354	10.88/10.31	$2H_2O$	Ru 29.10/28.93)
		467–551	510	30.17/31.23	$C_5H_7N_3$	
		552–720	640	29.88/29.22	$C_3H_2O_4$	
4	422.19	295–376	347	8.54/8.49	$2H_2O$	RuO 27.30/(27.59)
		459–505	500	37.55/37.73	$H_2P_2O_6$	
		506–999	770	26.61/25.70	$C_5H_7N_3$	

Table 6. The calculated quantum chemical parameters of Ru(II) complexes by DFT/B3LYP method and LanL2DZ basis set

Complex	HOMO, a.u	LUMO, a.u	η	ΔE, a.u	Electronic energy, a.u	D.M., Debye
2-Hydrazinopyridine	−0.216	−0.025	0.095	0.191	−359	1.46
1	−0.182	−0.056	0.063	0.126	−635	9.39
2	−0.181	−0.060	0.060	0.121	−982	14.27
3	−0.187	−0.060	0.059	0.118	−1022	14.00
4	0.073	0.167	0.047	0.094	−1145	13.27

[53].The calculation of atomic charges explains the potential donor and acceptor property of atoms [54]. The higher charge density in the 2-hydrazinopyridine ligand is allocated on nitrogen atoms of amine groups. This high charge explains their expected donor properties. Ruthenium has positive charge and acts as the acceptor atom. The increasing in the negative charges in the nitrogen atoms of the 2-hydrazinopyridine ligand in all complexes may be explain as MLCT from the ruthenium to the π* orbitals of the 2-hydrazinopyridine ligand. The dipole moment is an indicator of the polarity of molecules, the resulted data from calculations showed that the complexes are more polarized than the 2-hydrazinopyridine ligand. This is inferred from the values of the dipole moments (9.39–14.27 Debye) for complexes and (1.46 Debye) for the 2-hydrazinopyridine ligand [22–24].

The calculated electronic energy of the complexes as well as their dipole moments are tabulated in Table 6. The electronic energies of the complexes (−635 to −1145 a.u.) indicating that the complexes are more stable than the 2-hydrazinopyridine ligand (electronic energy = −359 a.u.) [22–24, 55]. The calculated HOMO and LUMO energies of the complexes **1**–**4** are given in Table 6. The hardness η values indicate the ease or difficulty to donate; it is calculated as $\eta = (I - A)/2$, where I is the ionization energy, A is the electron affinity, and $I - A$ is the gap between the HOMO and LUMO energy levels. The higher the value of $I - A$ the harder is the molecules and *vice versa* [56, 57]. The η values and ΔE (HOMO–LUMO) are given in Table 6.

The transition is easier in complexes as compared with the 2-hydrazinopyridine ligand as indicated from ΔE of complexes (0.094–0.126) to that of the 2-hydrazinopyridine ligand (0.191) and hence the complexes are softer (η = 0.047–0.063) than the 2-hydrazinopyridine ligand (0.095) [55]. The negative values of the HOMO and the LUMO energies in the complexes indicate their stability [55, 56, 58]. The isodensity surface plots of the HOMO and the LUMO for 2-hydrazinopyridine ligand and complex **1** are shown in Fig. 5. Natural Bond Orbital (NBO) calculations were performed [59]. According to NBO analysis for complex **1**, the electronic configuration of ruthenium is: [core] $5s^{0.22}\ 4d^{7.14}\ 5p^{0.15}\ 5d^{0.02}\ 6p^{0.34}$, 36 core electrons, 7.87 valence electrons, and 0.03 Rydberg electrons, which gives 43.90 total electrons and +0.132 e charge on ruthenium atom. The occupancies of ruthenium 4*d* orbitals are d_{xy} 1.33; d_{xz} 1.22; d_{yz} 1.09; $d_{x^2-y^2}$ 1.58 and d_{z^2} 1.92. The 4*d*-electron population of Ru(II) oxidation sate is 7.14 which indicates ligand-to-d_{Ru} electron

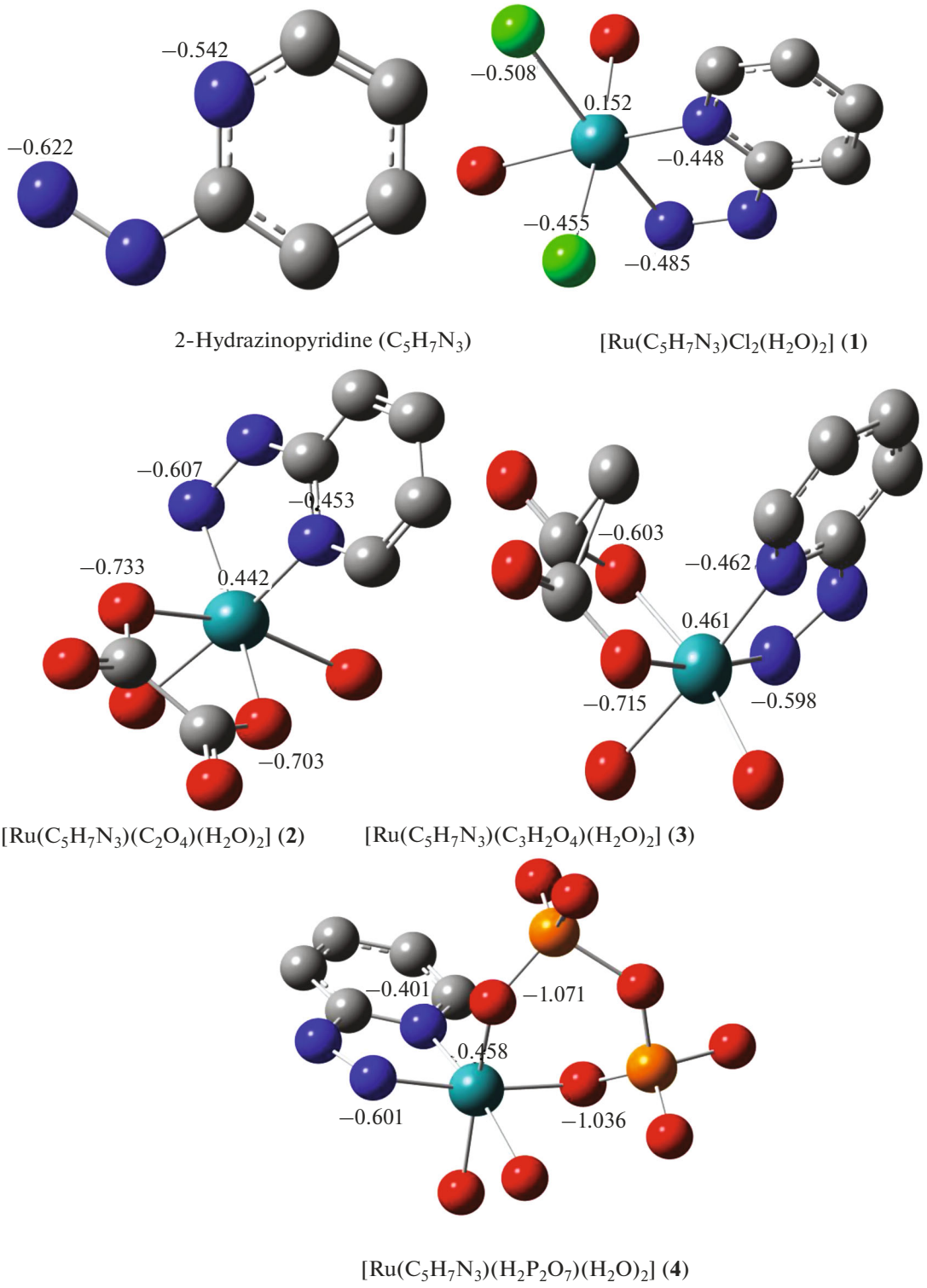

Fig. 4. Optimized molecular structure and atomic charges of Ru(II) complexes prepared; Carbon (gray), Nitrogen (blue), Chlorine (green), Oxygen (red), Phosphorous (orange) and Ruthenium (deep green). Hydrogen atoms are omitted.

transfer. Therefore, the natural charge of Ru(III) ion is reduced to Ru(II), which supports the higher complexation ability of the former ion towards ligand. Similar trends are shown by complexes **2**–**4** with Ru 4*d* populations 7.00–7.04 confirming the ligand-to-metal electron transfer [59].

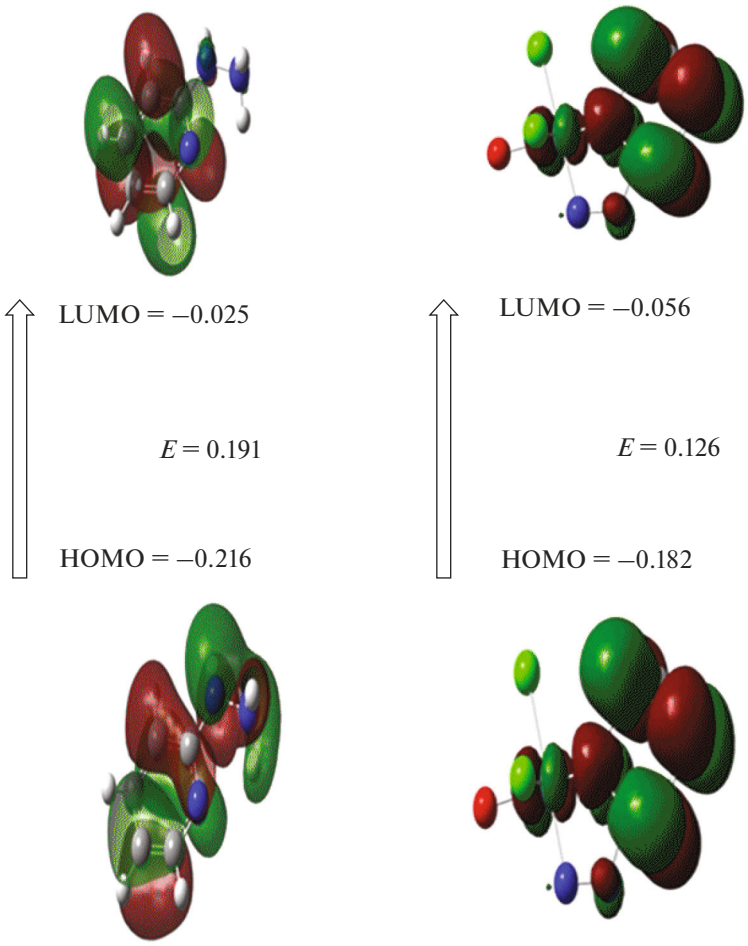

Fig. 5. The isodensity surface of 2-hydrazinopyridine ligand (left) and $[Ru(C_5H_7N_3)Cl_2(H_2O)_2]$ complex **1** (right) and energy splitting (isovalue 0.02).

The transition energy of the complexes has been calculated from TD-DFT (time-dependent density functional linear response theory). The electron densities in ligand are localized on the pyridine part which may point to a mixed $\pi \rightarrow \pi^*$ and $n \rightarrow \pi^*$ transition [56]. The energies of HOMO sates (H to H-4), the % contribution and the main characters of the 2-hydrazinopyridine ligand, Cl, ox, ma, PPi as well as ruthenium are calculated for complexes **1**–**4** and tabulated in Table S3 shown in SI. It has been found that in complex **1**, the % contribution of chloride to the HOMO states (H to H-4) varies in a wide range from 9 to 86% with the main character is Cl(π). On the other hand, the % contribution of chloride to LUMO states (L to L + 4) is much lower (0–14%). The % contribution of 2-hydrazinopyridine ligand in complex **1** to the HOMO states has been found to be low and varies from 4 to 8% through L(π) as the main character. The 2-hydrazinopyridine ligand % contribution to LUMO states has been found to be much higher than to the HOMO states and varies from 8 to 98% through L(π*) as the main character. Therefore, the electronic transition of the type $\pi \rightarrow \pi^*$ within complex **1** may be arisen from the HOMO states of high Cl(π) character to LUMO states with high L(π*) character. The ruthenium % contribution to the HOMO states varies from 2 to 6% by $Ru(t_{2g})$ as the main character (except H-1 and H-2 which have 84 and 81% contribution) through $Ru(t_{2g})$ and $Ru(e_g)$, respectively, which gives rise to the possibility of MLCT from $Ru(t_{2g})$ to either (Cl)(π*) and/or L(π*). On the other hand, the % contribution of Ru to the LUMO states varies from 2 to 47% (except L + 2 and L + 3 in which the contribution of Ru is 55%) which points to the possibility of LMCT from Cl(π*) and/or L(π*) to $Ru(e_g)$ [22–24, 55]. The % contribution and the main characters of Ru, Cl, ox, ma, PPi, and 2-hydrazinopyridine ligand to the different HOMO and LUMO states in complexes **2**–**4** showed more or less the same trend as complex **1**.

The molecular electrostatic potential (MEP) of complexes has been calculated and shown in Fig. 6,

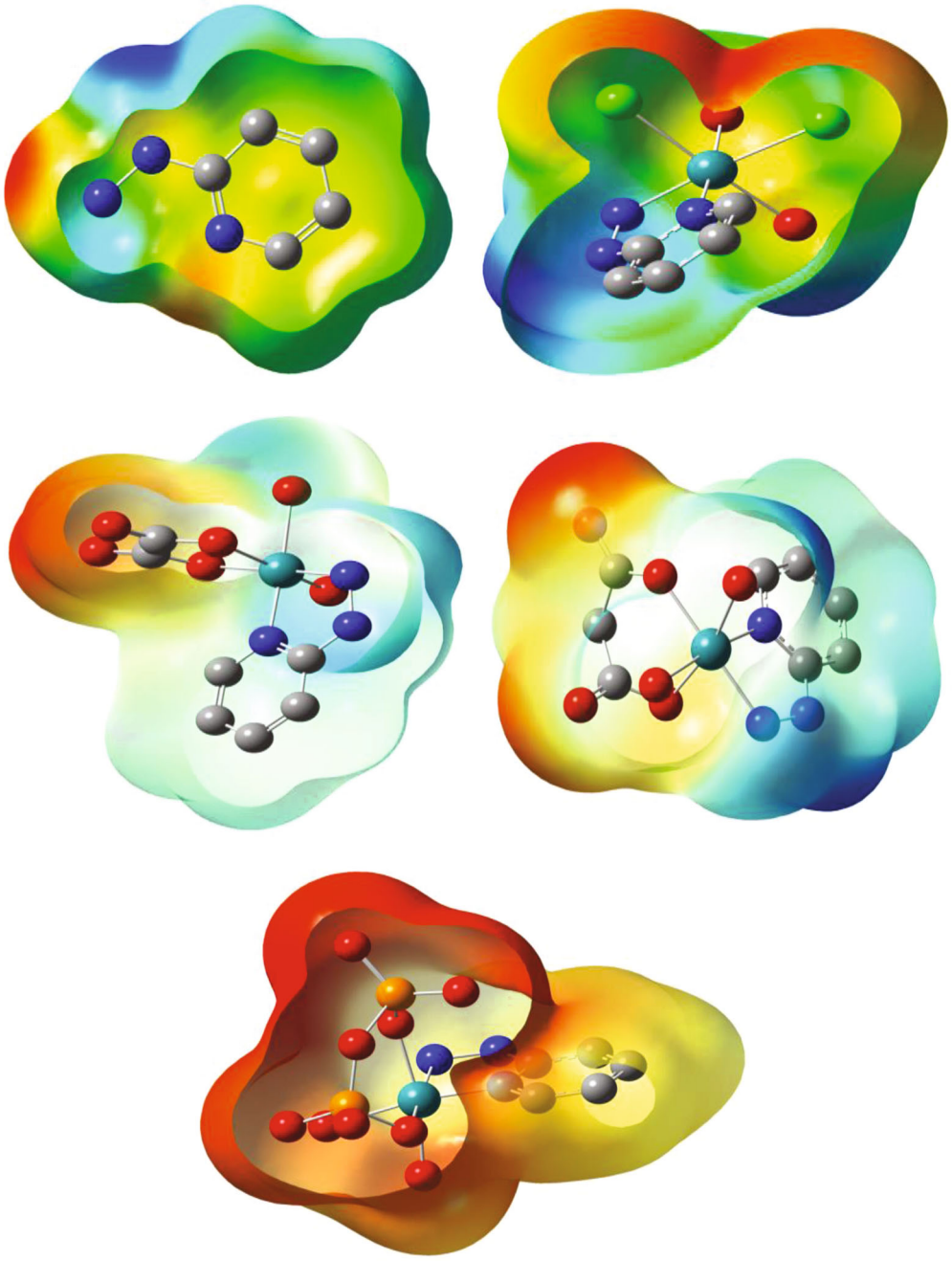

Fig. 6. Molecular electronic potential (MEP) of the 2-hydrazinopyridine ligand and Ru(II) complexes **1**–**4** (isocontour value = 0.0004) mapped with ESP. Hydrogen atoms are omitted for simplicity.

with the red regions indicate an electrophilic reactivity and the blue regions indicate a nucleophilic reactivity. The nitrogen atoms of the 2-hydrazinopyridine ligand with their negative (red) regions are the reactive sites for electrophilic attack [22–24]. On contrary, the negative (red) regions in complexes are mainly localized over the chlorine and oxygen atoms for oxalate, malate and pyrophosphate ligands.

In vitro Cytotoxicity

In vitro cytotoxic activities of the complexes **1**–**4** were determined in aqueous solutions against the HepG-2 (hepatocellular carcinoma cell line), MCF-7 (human breast adenocarcinoma cell line), PC-3 (prostate carcinoma cell line), and HTC-116 (colon carcinoma cell line). The IC_{50} values of the tested complexes are given in Table 7. The complexes have

Table 7. IC_{50} values of Ru(II) complexes

Complex	HepG-2	PC-3	HCT-116	MCF-7
1	0.027 ± 0.014	0.038 ± 0.012	0.012 ± 0.006	0.034 ± 0.004
2	0.071 ± 0.022	0.034 ± 0.011	0.136 ± 0.019	0.109 ± 0.008
3	0.078 ± 0.027	0.125 ± 0.008	0.134 ± 0.007	0.034 ± 0.006
4	0.088 ± 0.006	0.117 ± 0.004	0.154 ± 0.006	0.112 ± 0.007

good cytotoxicity with IC_{50} (μM) against HepG-2 (0.027–0.088), MCF-7 (0.034–0.112), PC-3 (0.034–0.125), and HCT-116 (0.012-0.154) cell lines (Figs. S21 and S22, see SI). The complexes are promising antitumor candidates because of their high solubility in water which may ease their injection and/or may enhance the chance of oral administration trial.

CONCLUSIONS

The complexes **1**–**4** have low spin and distorted octahedral geometry in which the2-hydrazinopyridine ligand acts as bidentate N2 donor. The distortion is indicated from the deviation of the angles around ruthenium atom from 90°. The energies of the HOMO and LUMO of the complexes were negative which indicate that the complexes are stable. The complexes are thermally stable as shown from their relatively high overall activation energies (101–254 kJ mol^{-1}). The complexes have good cytotoxicity with IC_{50} (μM) against HepG-2 (0.027–0.088), MCF-7 (0.034–0.112), PC-3(0.034–0.125) and HCT-116 (0.012–0.154) cell lines. The complexes are promising antitumor candidates because of their high solubility in water which may ease their injection and/or may enhance the chance of oral administration trial.

APPENDIX

Supplementary data associated with this article can be found in the online version. Supporting Information contains TGA data (Table S1), calculated geometric and energy parameters (Tables S2, S4), IR spectroscopy data (Figs. S1–S5), mass spectral data (Figs. S6–S9), electronic absorption data (Figs. S10–S13), calculated electronic transitions (Figs. S14–16), TGA data (Figs. S17–S20), and cytotoxicity data (Figs. S20, S21).

SUPPLEMENTARY MATERIAL

Supplementary materials are available for this article https://doi.org/10.1134/0.1134/S0036023619060020 and are accessible for authorized users.

REFERENCES

1. F. Barragán, P. López-Senín, L. Salassa, et al., J. Am. Chem. Soc. **133**, 14098 (2011). https://doi.org/10.1021/ja205235m
2. P. S. Kuhn, V. Pichler, A. Roller, et al., Dalton Trans. **44** (2), 659 (2015). https://doi.org/10.1039/C4DT01645A
3. S. Leijen, S. A. Burgers, P. Baas, et al., Invest. New Drugs. **33** (1), 201 (2015).
4. J. Iida, E. T. Bell-Loncella, M. L. Purazo, et al., J. Transl. Med. **14**, 48 (2016). https://doi.org/10.1186/s12967-016-0797-9
5. K. M. Deo, B. J. Pages, D. L. Ang, et al., Int. J. Mol. Sci. **17**, 1818 (2016). https://doi.org/10.3390/ijms17111818
6. L. Salassa, Eur. J. Inorg. Chem. **32**, 4931 (2011). https://doi.org/10.1002/ejic.201100376
7. S. Leijen, S. A. Burgers, P. Baas, et al., Invest. New Drugs. **33** (1), 201 (2015). https://doi.org/10.1007/s10637-014-0179-1
8. R. E. Aird, J. Cummings, A. A. Ritchie, et al., Br. J. Cancer. **86**, 1652 (2002). https://doi.org/10.1038/sj/bjc/6600290
9. L. Zeng, Y. Chen, Ji. Liu, et al., Sci. Rep. **6**, 19449(2016). https://doi.org/10.1038/srep19449
10. K. D. Mjos, and C. Orvig, Chem. Rev. **114**, 4540 (2014). https://doi.org/10.1021/cr400460s
11. J. F. Kou, C. Qian, J. Q. Wang, et al., J. Biol. Inorg. Chem. **17**,81 (2012). https://doi.org/10.1007/s00775-011-0831-6
12. F. Li, J. G. Collins, and F. R. Keene, Chem. Soc. Rev. **44**, 2529 (2015). https://doi.org/10.1039/C4CS00343H
13. H. Song, J. T. Kaiser, and J. K. Barton, Nat. Chem. **4**, 615 (2012). https://doi.org/10.1038/nchem.1375
14. A. Levina, A. Mitra, and P. A. Lay, Metallomics **1**, 458 (2009). https://doi.org/10.1039/b904071d
15. C. Qian, J. Q. Wang, C. L. Song, et al., Metallomics **5**, 844 (2013). https://doi.org/10.1039/c3mt20270d
16. T. A. Bhat, S. Kumar, A. K. Chaudhary, et al., Drug Discovery Today. **20**, 635 (2015).
17. S. F. Georg, Dalton Trans. **39**, 1673 (2010). https://doi.org/10.1039/B916860P
18. O. A. Lenis-Rojas, A. R.Fernándes, C. R. Rodrigues, et al., Dalton Trans. **45,** 19127 (2016).

19. R. H. Berndsen, A. Weiss, U. K. Abdul, et al., Sci. Rep. **22** (7), 43005 (2017). https://doi.org/10.1038/srep43005
20. C. S. Allardyce, and P. J. Dyson, Dalton Trans. **45**, 3201 (2016). https://doi.org/10.1039/c5dt03919c
21. L. Salassa et al., Organometallics **29**, 6703 (2010), https://doi.org/10.1021/om100734y
22. A. A. Soliman, O. I. Alajrawy, F. A. Attabi, and W. Linert, New J. Chem. **40**, 8342 (2016). https://doi.org/10.1039/C6NJ01262K
23. A. A. Soliman, O. I. Alajrawy, F. A. Attabi, and W. Linert, Spectrochim. Acta A. **152**, 358 (2016).
24. A. A. Soliman, O. I. Alajrawy, F. A. Attabi, et al., J. Mol. Struct. **1115**, 17 (2016).
25. M. M. Elaasser, M. M. Abdel-Aziz and R. A. El-Kassas, J. Microbiol. Biotech. Res. **1** (4), 5 (2011).
26. P. S. Hallman, T. A. Stephenson, and G. Wilkinson, Inorg. Synth. **12**, 237 (1970).
27. J. A. Broomhead, and C. G.Young, Inorg. Synth. **28**, 338 (1990).
28. A. T. Vu, D. A. Santos, J. G. Hale, and R. N. Garner, Inorg. Chim. Acta **450**, 23 (2016).
29. B. P. Sullivan, D. J. Salmon, and T. J. Meyer, Inorg. Chem. **17** (12), 3334 (1978).
30. A. A. Soliman, M. A. Amin, A. A. El-Sherif, et al., Arab. J. Chem. **10**, 389 (2017).
31. N. Nakamoto, *Infrared and Raman Spectra of Inorganic and Coordination Compounds* (New York, Wiley, 1986).
32. B. S. Kim, S. H. Kim, Y. S. Kim, S et al., Mol. Cryst. Liquid Cryst. **504**, 173 (2009).
33. H. Bih, I. Saadoune, and M. Mansori, J. Conden. Mater. **7** (1), 74 (2006).
34. Y. Makhkhas, S. Aqdim, and E. Sayouty, J. Mater. Sci. Chem. Engineer. **1**, 1 (2013).
35. R. Essehli, B. El Bali, M. Lachkar, et al., Acta Cryst. **62**, 538 (2006).
36. N. G. Armatas, G. D. Allis, A. Prosvirin, et al., Inorg. Chem. **47**, 832 (2008).
37. R. P. Bush, Platinum Met. Rev. **35** (4), 202 (1991).
38. C. Sahin, A. Goren, and C. Varlikli, Synthesis, J. Organomet. Chem. **772–773**, 68 (2014). https://doi.org/10.1016/j.jorganchem.2014.08.031
39. A. B. P. Lever, *Inorganic Electronic Spectroscopy*, 2nd ed. (Elsevier, Amsterdam, 1984).
40. G. C. Pellacani, and W. D. D. Malavasi, J. Inorg. Nucl. Chem. **37**, 477 (1975).
41. R. A. Palmer, and T. S. Piper, Inorg. Chem. **5**, 864 (1966).
42. C. E. Housecroft, and A. G. Sharpe, *Inorganic Chemistry*, 2nd ed. (Pearson, England, 2005).
43. A. A. Soliman, M. M. Khattab, and R. M. Ramadan, Trans. Met. Chem. **32**, 325 (2007).
44. S. A. Ali, A. A. Soliman, M. M. Aboli, and R. M. Ramadan, J. Coord. Chem. **55**, 1161 (2002).
45. H. H. Horowitz, and G. Metzger, Anal. Chem. **35** (10), 1464 (1963).
46. A. W. Coats, and J. P. Redfern, Nature **201**, 68 (1964).
47. A. A. Soliman, M. E. Samir, and A. M. Omyma Ali, J. Therm. Anal. Calorim. **83**, 385 (2006).
48. C. Lee, W. Yang, and R. G. Parr, Phys. Rev. B **37**, 785 (1988).
49. R. Robinson, Jr., K. K. Abbasi, A. Ariafard, et al., Inorg. Chem. **54** (2), 534 (2015). https://doi.org/10.1021/ic502298j
50. F. Caruso, M. Rossi, A. Benson, et al., J. Med. Chem. **55**, 1072 (2012).
51. I. Warad, M. Al-Noaimi, O. S. Abdel-Rahman, et al., Spectrochim. Acta A **117**, 250 (2014).
52. S. D. Inglez, F. C. A. Lima, M. R. Camilo, et al., J. Braz. Chem. Soc. **21**, 157 (2010).
53. S. H. Dale, and M. R. J. Elsegoodb, Acta Cryst. C **62**, 166 (2006).
54. R. Robinson Jr., M. F. Shaw, R. Stranger, and B. F. Yates, Dalton Trans. **45**, 1047 (2016). https://doi.org/10.1039/c5dt03600c
55. A. C. Tsipis, Coord. Chem. Rev. **272**, 1 (2014). . https://doi.org/10.1016/j.ccr.2014.02.023
56. S. J. Sabounchei, P. Shahriary, S. Salehzadeh, et al., Spectrochim. Acta A **135**, 1019 (2015).
57. L. Mazur, B. Modzelewska-Banachiewicz, R. Paprocka, et al., J. Inorg. Biochem. **114**, 55 (2012).
58. F. Neese, Coord. Chem. Rev. **253**, 526 (2009).
59. A. M. Mansour, Inorg. Chim. Acta. **394**, 436 (2013).